Controlling and Manipulating Confined Infrared Light in MoO_3 via Polaritonic Design

Ethan D. Ray[1], Saurabh Dixit[2], Mingze He[2], Ryan Kowalski[2], Joshua D. Caldwell[2]
[1]Department of Materials Science and Engineering, Georgia Institute of Technology, Atlanta, GA
[2]Department of Mechanical Engineering, Vanderbilt University, Nashville, TN

Background & Motivation

- Infrared (IR) radiation is crucial for studying long-wave thermal energy
- IR light detects thermal fingerprints of molecules using unique lattice vibrations [1]
- Spatial resolution of IR optics is limited due to their long free-space wavelengths [2]

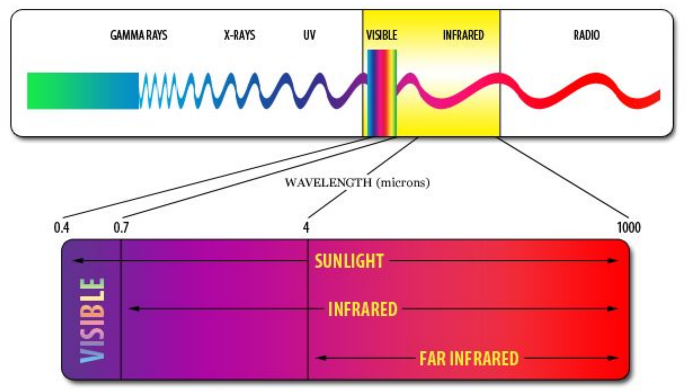

- Sub-diffractional confinement of IR light opens the door to novel sensing, communication, & imaging devices

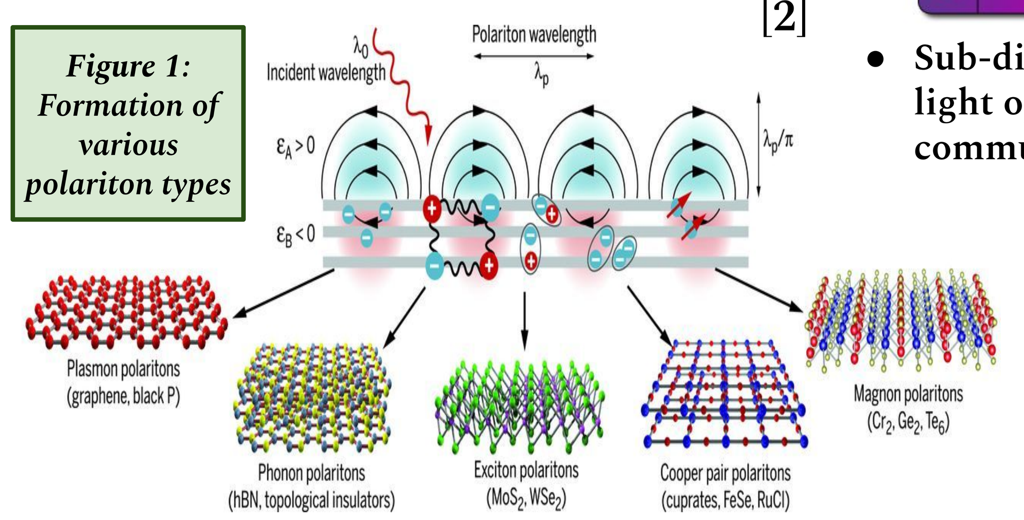

Figure 1: Formation of various polariton types

- Quasi-particles known as phonon polaritons (PhPs) have been shown to compress light to such dimensions
- PhPs are quasi-particles of coherent oscillating charges coupled with photons (light) [3]
- Hyperbolic materials - dielectric permittivities that are opposite in sign along different directions
- Such materials support HPhPs (HPhPs) w/ frequency-dependent propagation directions
- α-MoO_3 exhibits hyperbolicity both in- and out-of-plane

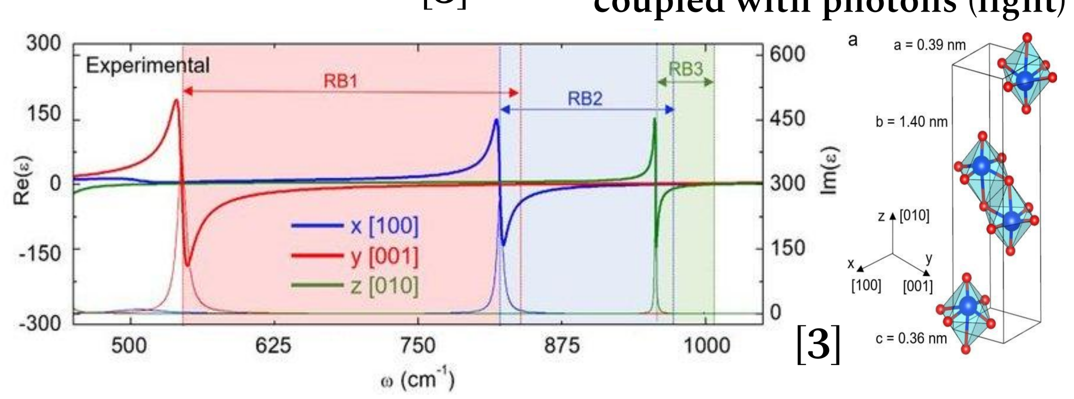

Figure 2: a) Dielectric function of MoO_3 with three Restrahlen bands (RB1, RB2, and RB3) b) Orthorhombic crystal structure of MoO_3 drives optical anisotropy

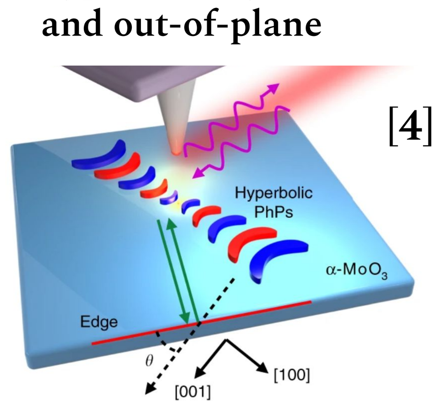

[4]

Figure 3: Propagation and edge interactions of HPhPs in MoO_3 slab

- Propagation behavior and wavelengths of HPhPs (λ_p) can be tuned and confined using sub-wavelength structures of α-MoO_3 crystals
- Light scattering from α-MoO_3 structures stimulates HPhP standing waves that result in a strong resonance
- Sub-wavelength wedge structures offer distinct opportunities in confining and focusing HPhPs due to physical tapering

Experiment Overview

- In sub-wavelength wedges, polaritonic modes are expected to undergo topological transitions
- Changing wedge vertex angles (θ_v) can be used to induce transitions in polaritonic modes and propagation characteristics
- COMSOL simulations used to optimize geometry and define propagation phenomena before fabrication and experimental study

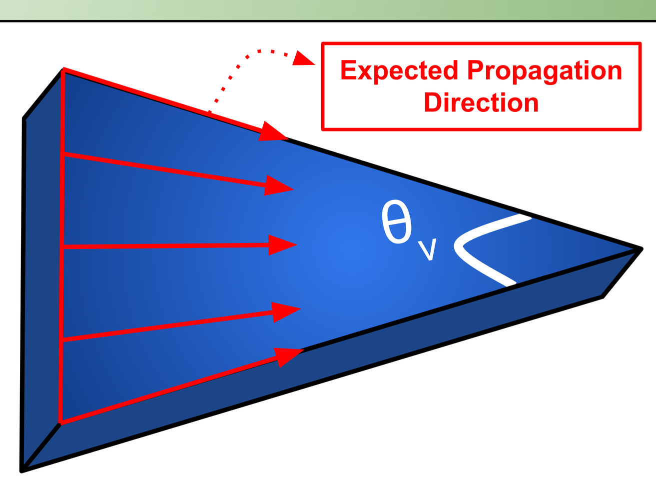

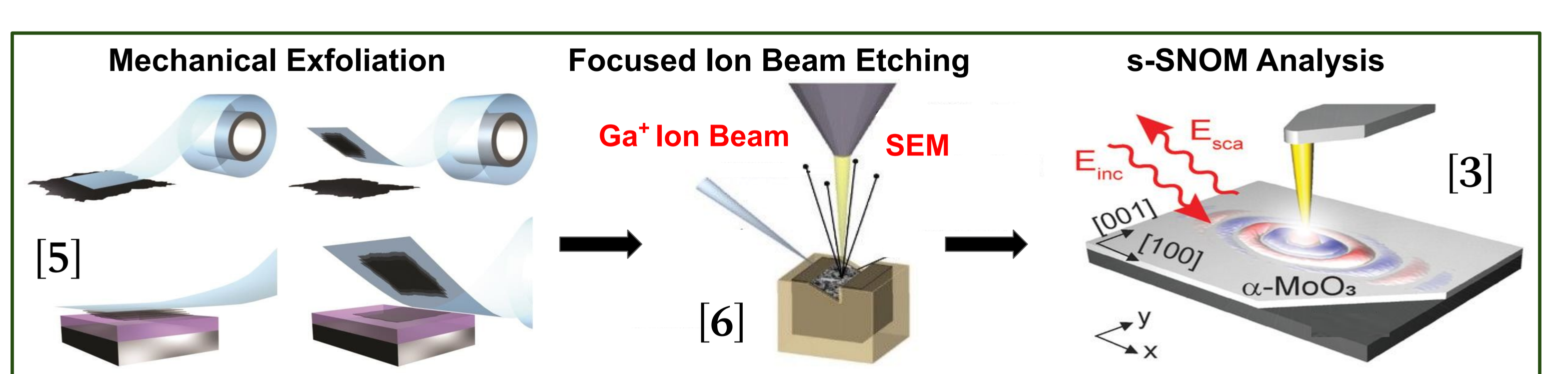

Figure 4: Procedure for the fabrication and polaritonic testing of MoO_3 wedge structures

Sub-Wavelength MoO_3 Wedges

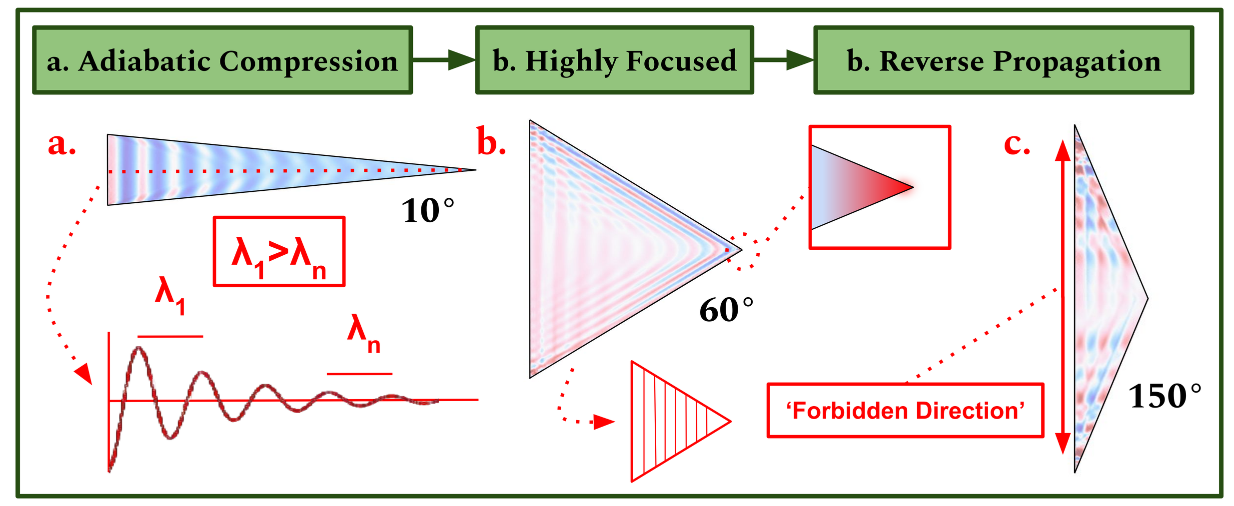

Figure 5: Three distinct propagation modes within 10° < θ_v < 150°

a) Acute θ_v → Adiabatically compressed waves (edges bend resonances inward)

b) Intermediate θ_v → Highly focused standing waves

c) Obtuse θ_v → Reversed propagation waves

Adiabatic Compression Transition

RB1 Propagation

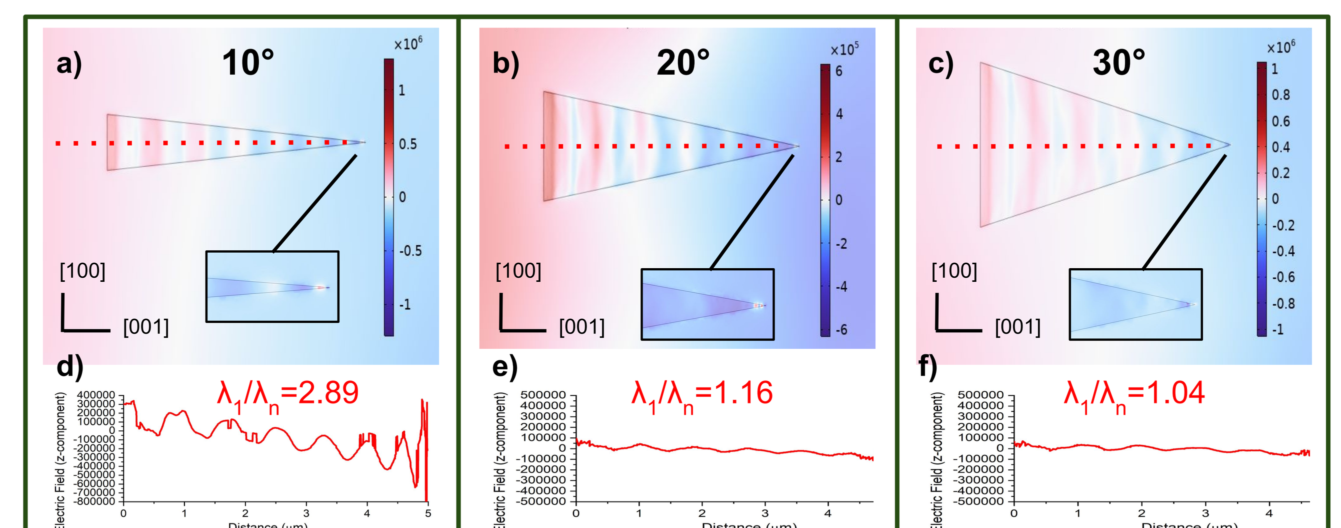

Figure 6: (a-c) Acute wedge geometries with [001] propagation at frequency of 700.48cm^{-1} (d-f) Near-field profiles along [001] from base to apex on wedge surfaces

RB2 Propagation

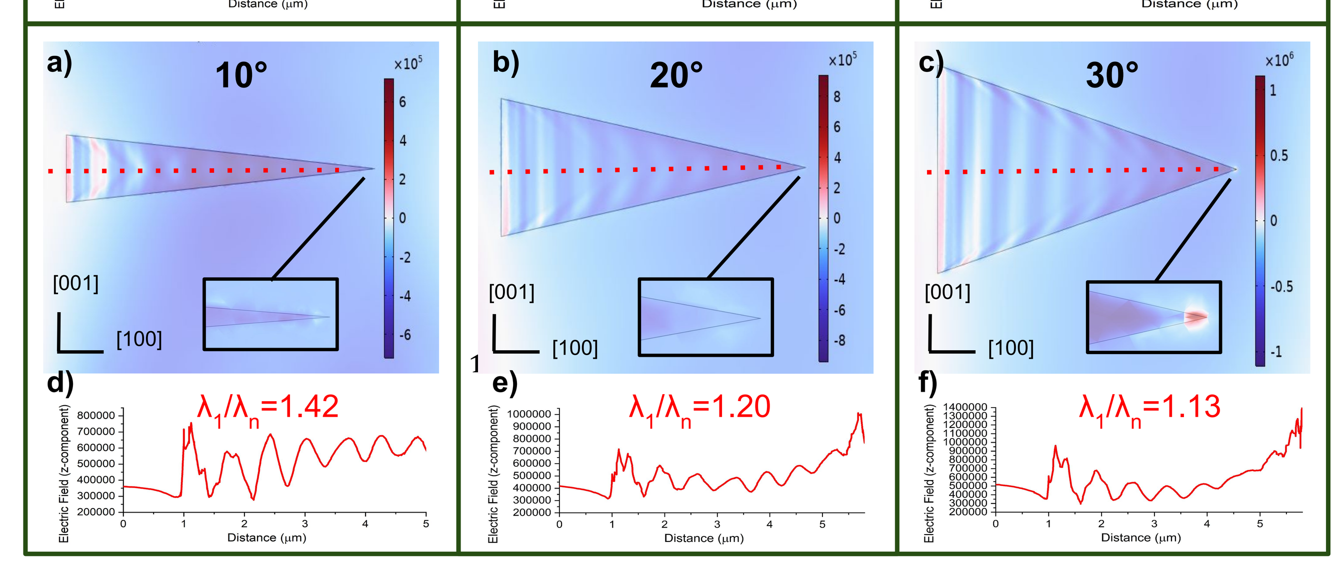

Figure 7: (a-c) Acute wedge geometries with [100] propagation at a frequency of 900.61cm^{-1} (d-f) Near-field profiles along [100] from base to apex on wedge surfaces

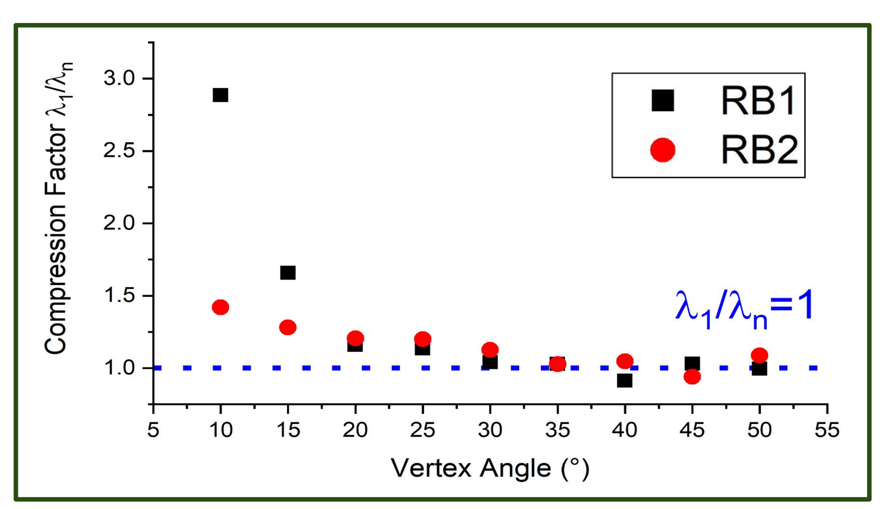

Transition to Highly Focused Behavior

Figure 8: Comparison of adiabatic compression transition for RB1 and RB2 propagation in acute wedges (10°- 50°) via compression factor (λ_1/λ_n) analysis with full transition at λ_1/λ_n=1

Reverse Propagation Transition

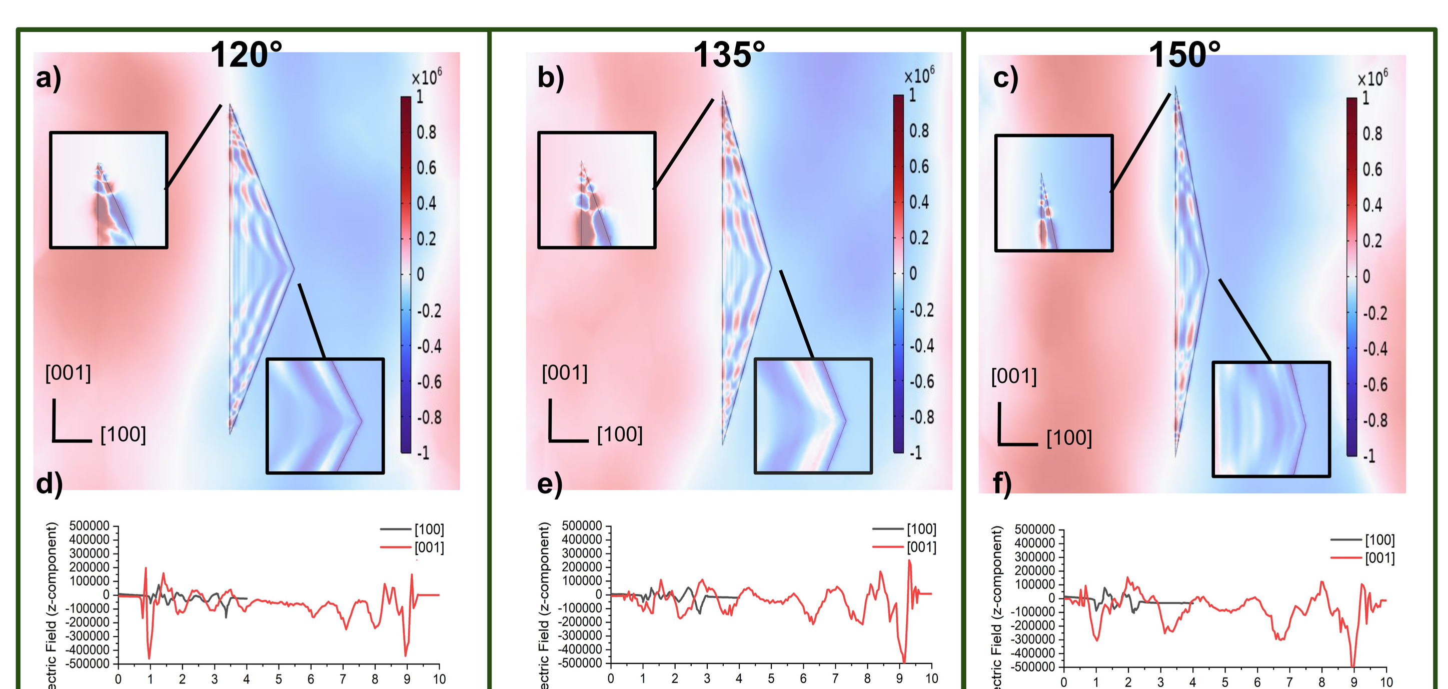

Figure 9: (a-c) Obtuse wedge geometries with [100] and [001] propagation at a frequency of 900.61cm^{-1} (d-f) Near-field surface profiles along [100] from base to apex on wedge and [001] 'forbidden direction'

Conclusions & Outlook

- Formation of three wedge propagation states form at various θ_v ranges
  - Adiabatic compression is increasingly dominated by standing wave resonance up to ~30° and reverse propagation behavior increases in the 120° < θ_v < 150°
- High energy profile confinement to apex achieved within 1.0<λ_1/λ_n<1.2
  - Engineering of λ_1/λ_n can be used to induce high focusing at apex
- Adiabatic compression within RB1 and RB2 both settled at ~30°, however at unique rates due to $\lambda_{p,RB2}$ > $\lambda_{p,RB1}$ at the HPhP launch site
  - Intrinsic biaxial property of MoO_3 dielectric permittivity tensor
- Realization of 'forbidden direction' propagation in obtuse sub-wavelength wedges
  - Similar effect seen in nano-ribbons of similar dimensions and conditions within RB2 (He et al., 2023)
  - Wavenumber and width along [100] combination consistent with nano-ribbon work (He et al., 2023)
- Symmetry of 'forbidden propagation' witnessed in [001] direction
  - Multi-directional focusing applications

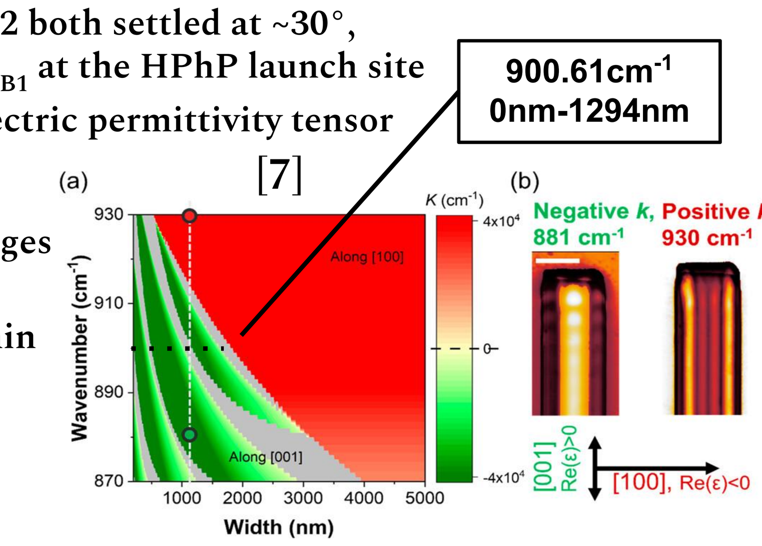

Figure 10: Modified figure (He et al., 2023) a) frequency and nano-ribbon width combinations for reverse propagation (green), normal propagation (red), and no propagation (gray) b) Visualization of reversed vs. normal propagation

Future Work

- Experimental testing of all three propagation mode conditions
- s-SNOM: the scattering of light off of a fine tip allows for near-field light-matter interactions to be probed and mapped over a defined area
- More precise angle-dependence sweeps and relations (angle-by-angle changes)
- Other geometric parameters of study (thickness dependence, orientational skew, etc.)

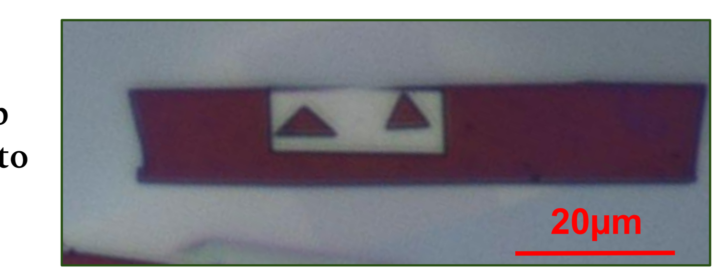

Figure 11: Optical image of sub-wavelength wedge samples fabricated through mechanical exfoliation and FIB etching

[8]

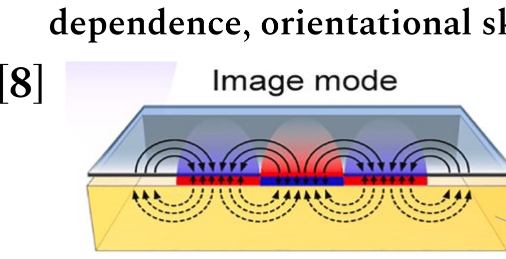

- Image Polariton Effect: perfect electric conductor with a polaritonic material creates a mirror-polariton that couples with the original (Menabde et al., 2022)

References & Acknowledgements

Special thanks to VINSE, Jamie Kuntz, and Sarah Ross for supporting me in the development of this work. Thank you to the Caldwell Nanophotonic Materials and Devices Lab, specifically Courtney Ragle, Mackey "Trey" Long III, Megan Dernberger, William Ford, and Ella Dzialowski for technical aid throughout the duration of the project. Sincerest gratitude to Taylor Baugher, Shereena Johnson, Ellie Okonak, and Jacqueline Anatot for personal support for this project. Finally, thank you to the National Science Foundation for funding and making this work possible. (Grant: **NSF-DMR 1852157**)

[1] History of Infrared & Infrared Technology. BioSmart Solutions

[2] Basov, D. N., et al. "Polaritons in van Der Waals Materials." Science, vol. 354, no. 6309, 2016, doi.org/10.1126/science.aag1992

[3] Álvarez-Pérez, Gonzalo, et al. "Infrared Permittivity of the Biaxial van Der Waals Semiconductor α-MoO_3 from Near- and Far-field Correlative Studies." Advanced Materials, vol. 32, no. 29, 2020, p. 1908176, doi.org/10.1002/adma.201908176

[4] Dai, Zhigao, et al. "Edge-Oriented and Steerable Hyperbolic Polaritons in Anisotropic van Der Waals Nanocavities." Nature Communications, vol. 11, no. 1, 2020, doi.org/10.1038/s41467-020-19913-4

[5] Liu, Xinling, et al. "Thin-Film Electronics Based on All-2d van Der Waals Heterostructures." Journal of Information Display, vol. 22, no. 4, 2021, pp. 231–245, doi.org/10.1080/15980316.2021.1982782

[6] Focused ion beam/scanning electron microscope. Wisconsin Centers for Nanoscale Technology.

[7] He, Mingze, et al. "Guided Polaritons along the Forbidden Direction in MoO_3 with Geometrical Confinement." Nano Letters, vol. 23, no. 11, 2023, pp. 5035–5041, doi.org/10.1021/acs.nanolett.3c00892

[8] Menabde, Sergey G., et al. "Image Polaritons in van Der Waals Crystals." Nanophotonics, vol. 11, no. 11, 2022, pp. 2433–2452, doi.org/10.1515/nanoph-2021-0693.